Supplementary information for:

Drygalski Ice Tongue stability influenced by rift formation and ice morphology

Christine Indrigo, Christine Dow, Jamin Greenbaum, Mathieu Morlighem

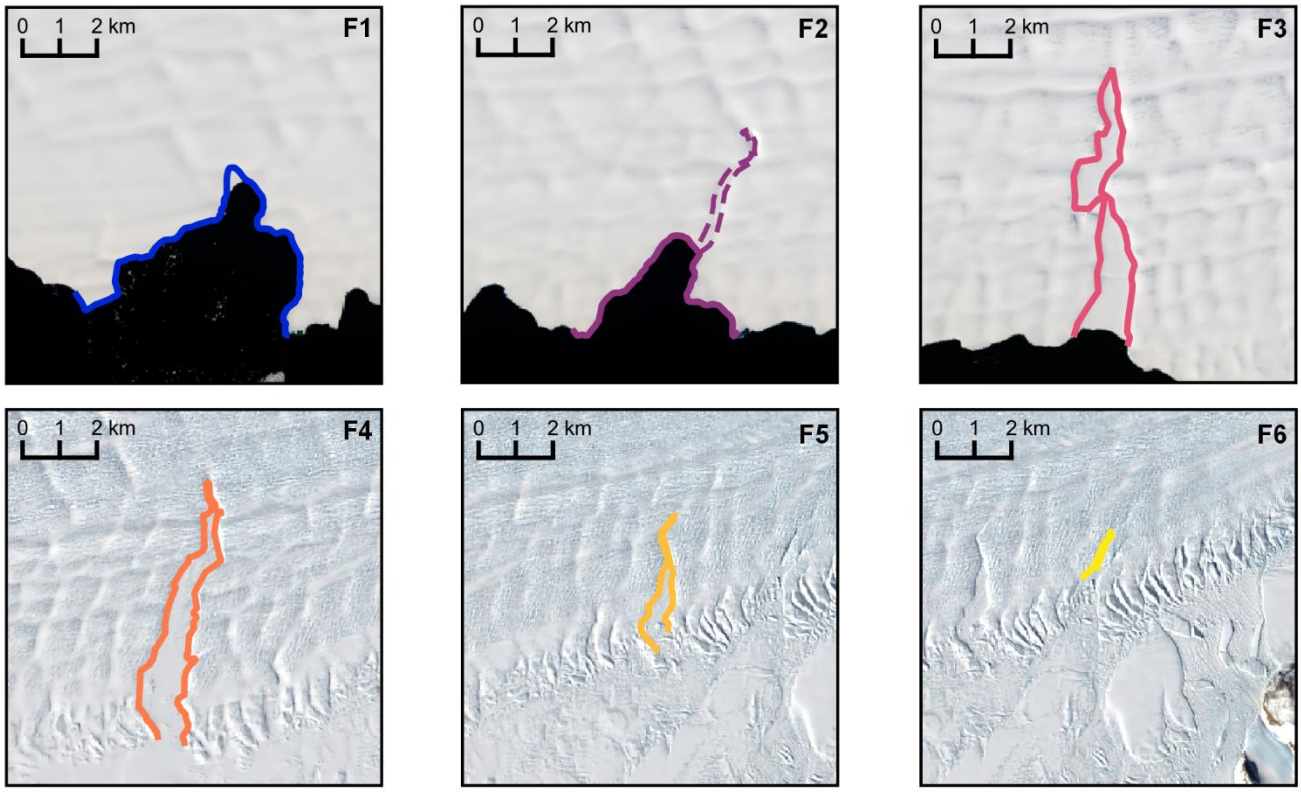

Figure S1. Outlines of the 6 large fractures over a 30 December 2017 Landsat 8 image. Solid line for F2 indicates the rift outline, dashed line indicates the fracture outline.

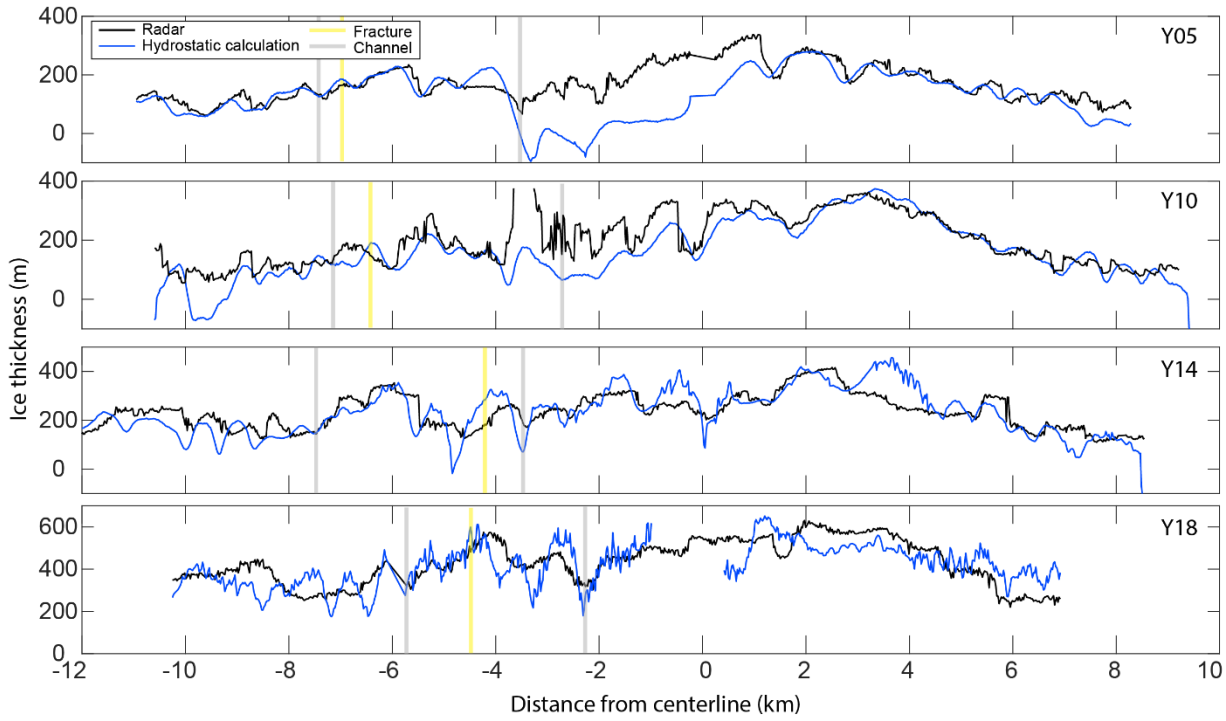

Figure S2. Ice thickness profiles for Y05, Y10, Y14 and Y18 from radar (black line) and from our hydrostatic calculations extracted from REMA surface DEM (blue line). Locations of basal channels are plotted with the gray lines. Extrapolated location of the nearest fracture is shown with the yellow line. For locations of these profiles, see Fig. 2c in the main manuscript.

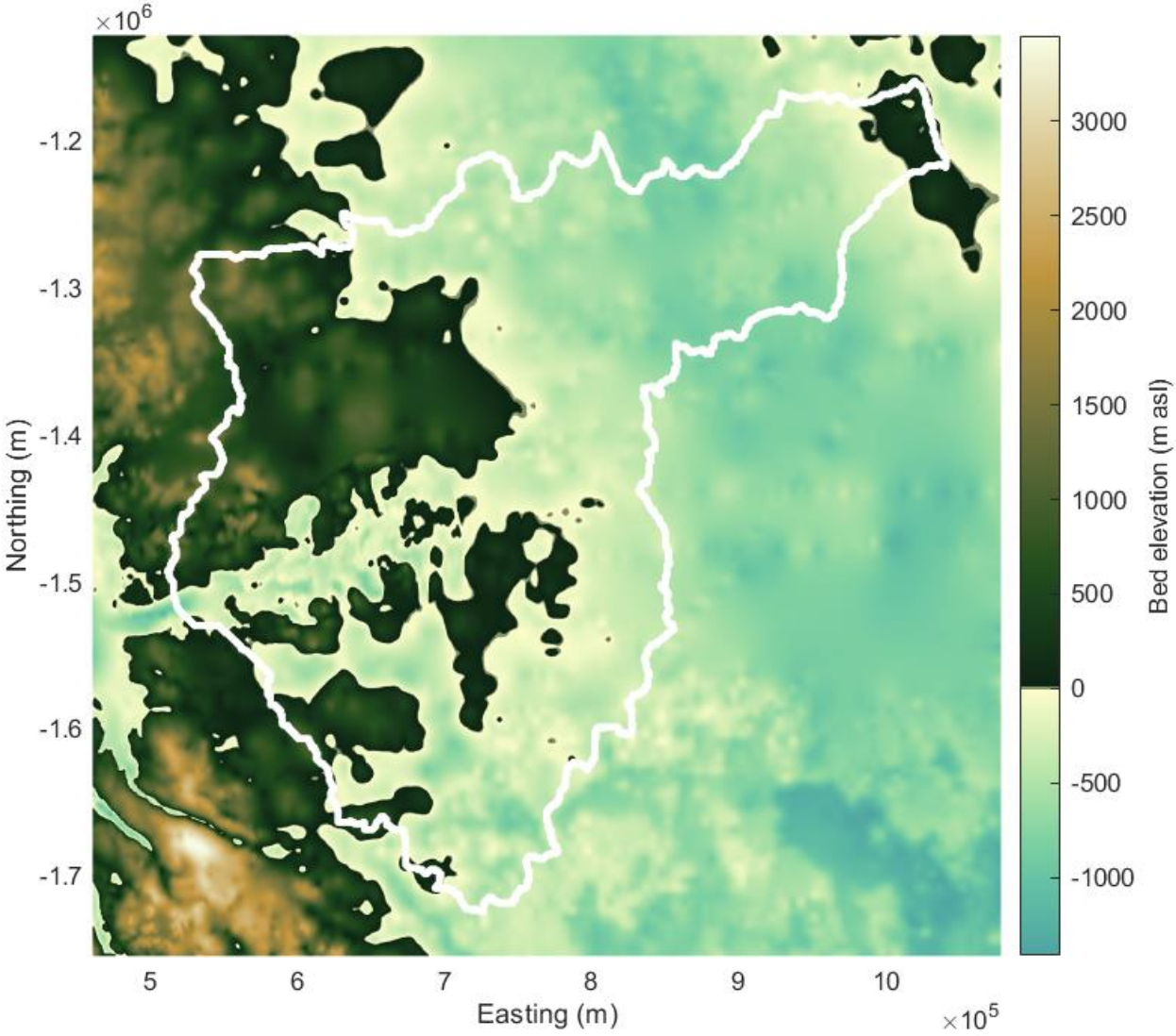

Figure S3. Bed elevation (m asl) of the David Glacier catchment from BedMachine with the GlaDS model domain outlined in white.

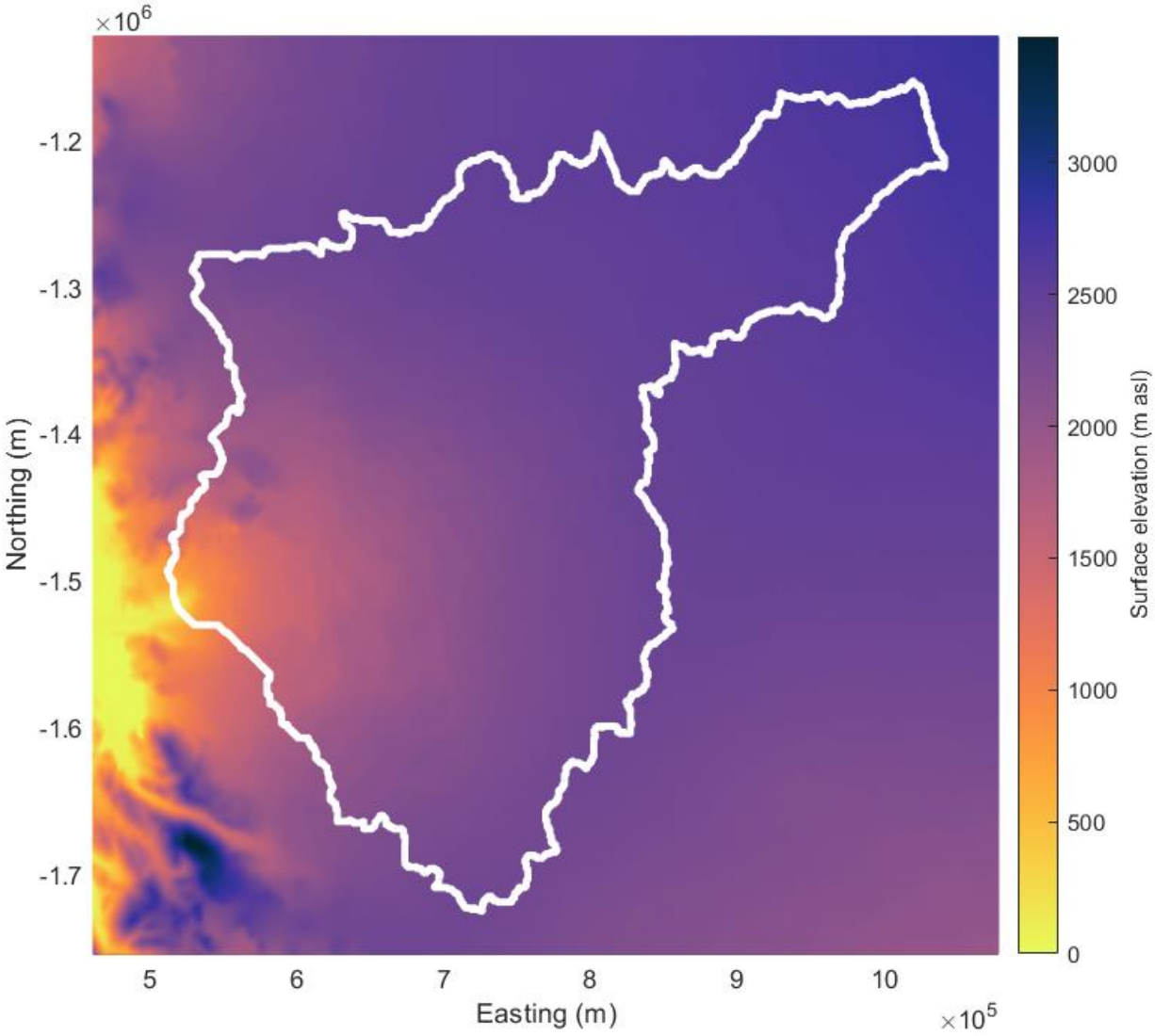

Figure S4. Surface elevation (m asl) of the David Glacier catchment from BedMachine with the GlaDS model domain outlined in white.

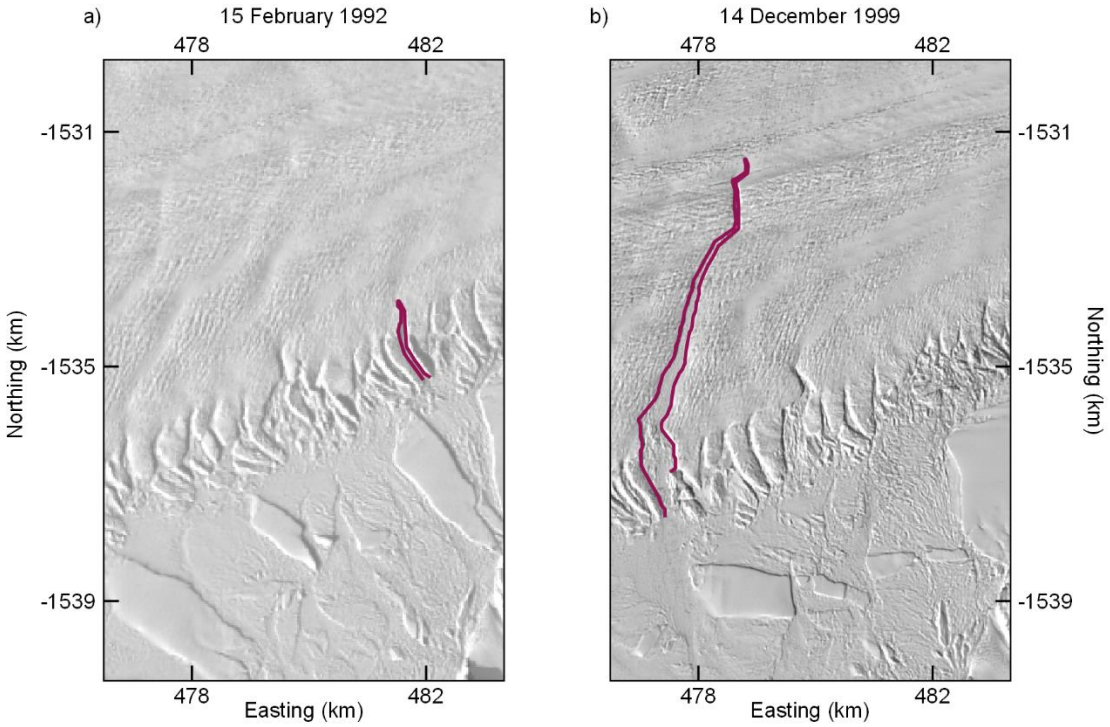

Figure S5. Image showing the formation and growth of the F4 fracture. Left: outline of the fracture in 1992. Right: outline of the fracture in 1999. Image source: Landsat 4 TM path 63 row 113, acquisition date: 15 February 1992 (left); Landsat 7 ETM+ path 63 row 113, acquisition date: 14 December 1999 (right).

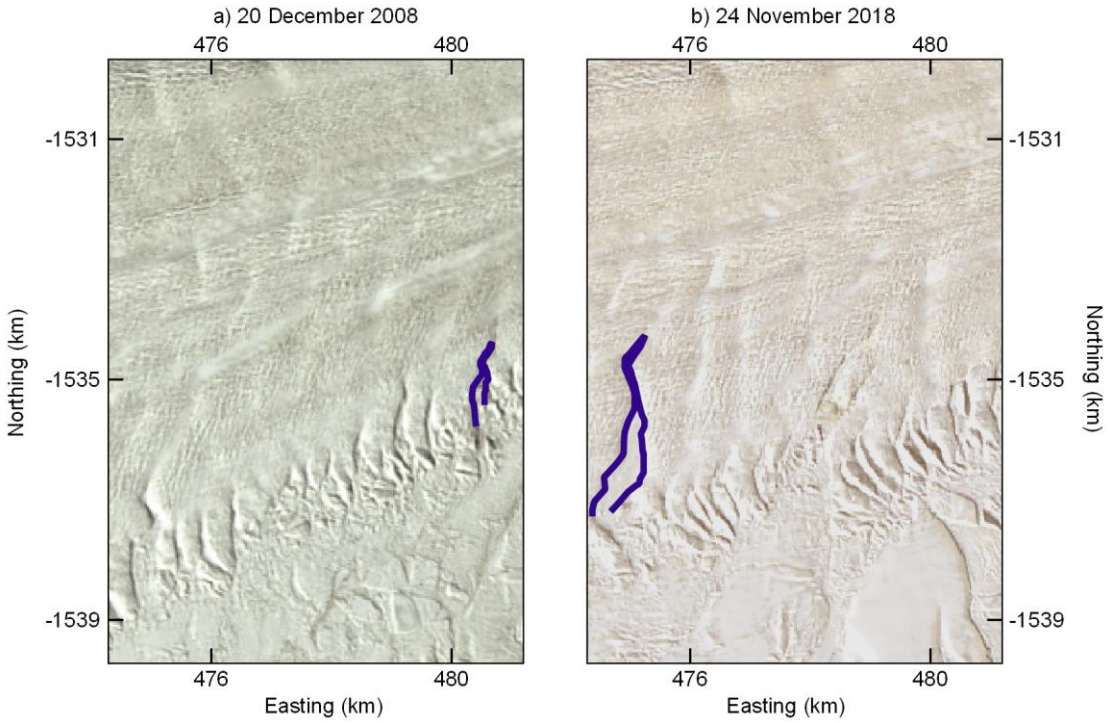

Figure S6. Image showing the formation of the F5 fracture. Left: outline of the fracture in 2008. Right: outline of the fracture in 2018. Image source: Landsat 7 ETM+ path 62 row 113, acquisition date: 20 December 2008 (left); Landsat 8 OLI/TIRS path 60 row 114, acquisition date: 24 November 2018 (right).

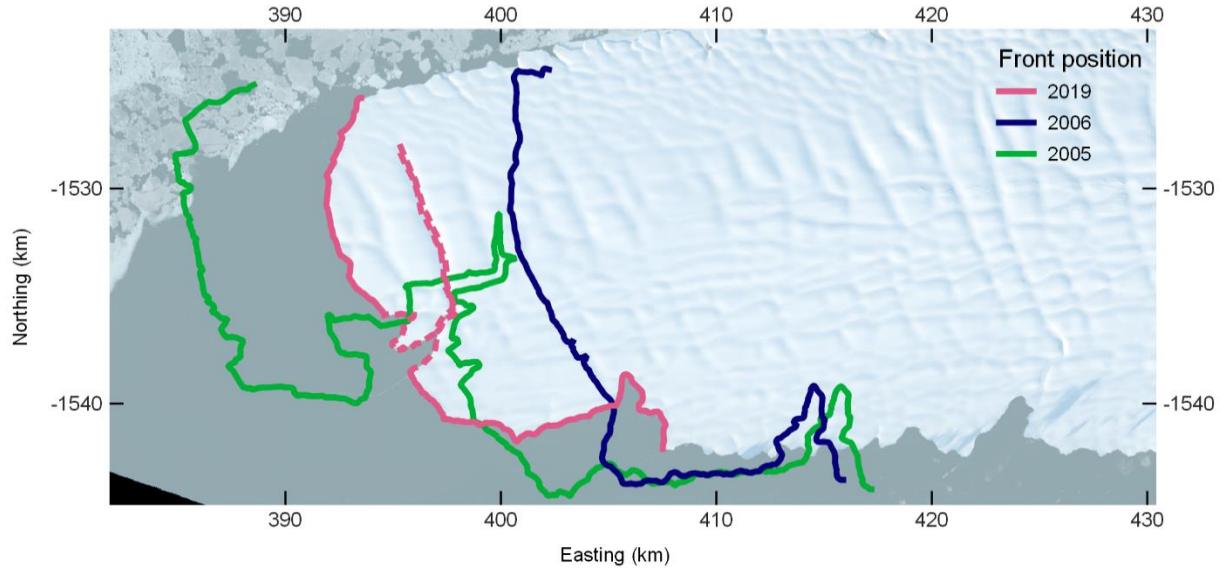

Figure S7. Drygalski Ice Tongue calving front outlines on 28 January 2005 (green), 17 December 2006 (dark blue), and 23 May 2019 (pink). The dashed pink line indicates the rifting section of the calving front in 2019. The 2005 outline is before the large 2005-2006 calving event, and the 2006 outline is after this event. Image source: Landsat 8 OLI/TIRS path 60 row 114, acquisition date: 24 November 2018.

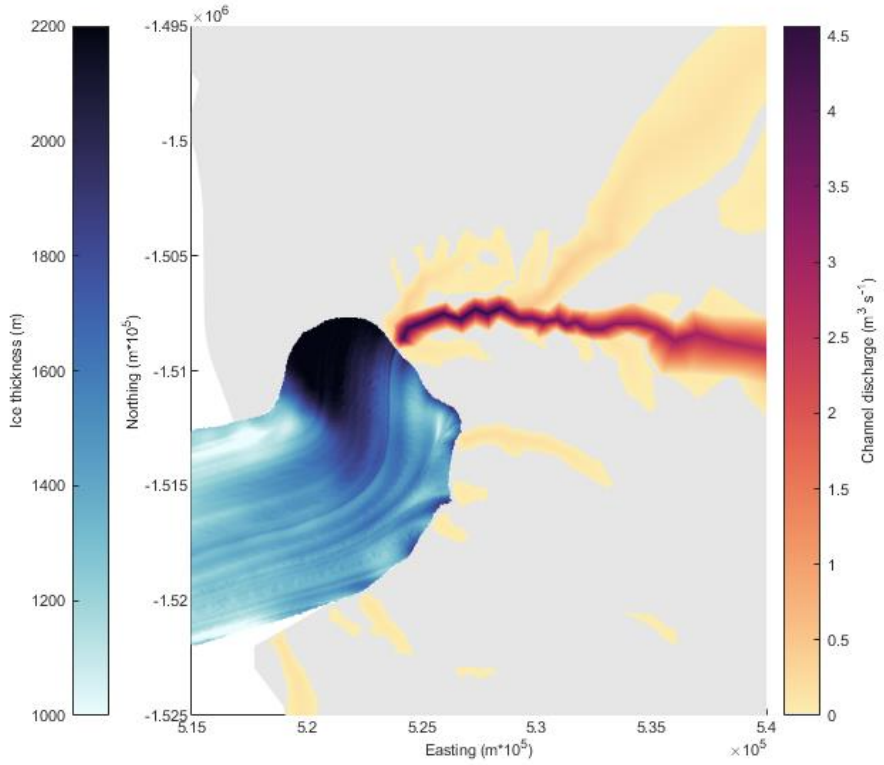

Figure S8. Channel discharge from GlaDS (Model Run 5 in Table S4) plotted with Drygalski Ice Tongue ice thickness identified using remote sensing imagery. Ice thickness (m) derived from REMA, from white (1000 m) to blue (2200), and channel discharge modelled in GlaDS, from yellow (0 m^3 s^{-1}) to purple (4.5 m^3 s^{-1}).

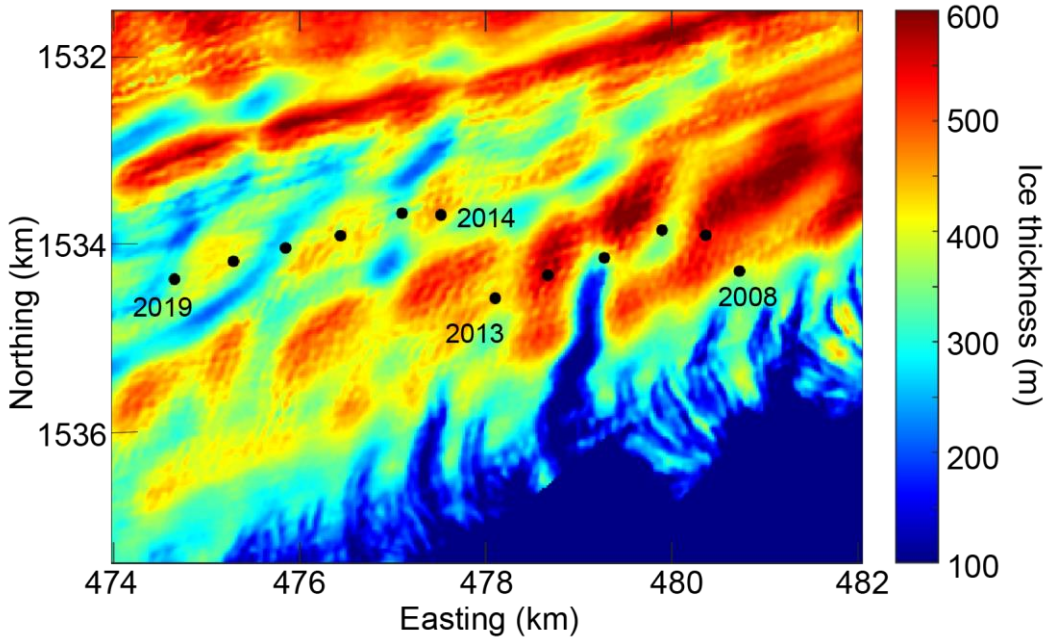

Figure S9. Fracture F5 tip location plotted annually from 2008 to 2019 (black dot). The background image is hydrostatic thickness calculated from REMA surface elevation data. As REMA is only representing a temporally static thickness there will be some error in the thickness estimates relative to the fracture location. The fracture can be seen in the thickness map at its 2011 position.

Table S1. Landsat images used in this study.

Scene ID	Acquisition Date	Satellite	Sensor	Resolution
LT04_L1GS_060114_19881215_20170205_01_T2_B4	15 December 1988	Landsat 4	TM	30 m
LT04_L1GS_062113_19890303_20170204_01_T2_B1	3 March 1989			
LT04_L1GS_062113_19900117_20170131_01_T2_B3	17 January 1990			
LT04_L1GS_063113_19920215_20170124_01_T2_B1	15 February 1992			
LT05_L1GS_062113_19910128_20170127_01_T2_B3	28 January 1991	Landsat 5	TM	30 m
LE07_L1GT_060114_19991230_20170215_01_T2_B8	30 December 1999	Landsat 7	ETM+	15 m
LE07_L1GT_059114_20000124_20170213_01_T2_B8	24 January 2000			
LE07_L1GT_061113_20010209_20170207_01_T2_B8	9 February 2001			
LE07_L1GT_061113_20011226_20170201_01_T2_B8	26 December 2001			
LE07_L1GT_060114_20020104_20170201_01_T2_B8	4 January 2002			
LE07_L1GT_062113_20021204_20170127_01_T2_B8	4 December 2002			
LE07_L1GT_061113_20030114_20170127_01_T2_B8	14 January 2003			
LE07_L1GT_060114_20050128_20170116_01_T2_B8	28 January 2005			
LE07_L1GT_060114_20061217_20170106_01_T2_B8	17 December 2006			
LE07_L1GT_061114_20071211_20170101_01_T2_B8	11 December 2007			
LE07_L1GT_060114_20081120_20161224_01_T2_B8	20 November 2008			
LE07_L1GT_060114_20081206_20161224_01_T2_B8	6 December 2008			
LE07_L1GT_061114_20091216_20161218_01_T2_B8	16 December 2009			
LE07_L1GT_060114_20101212_20161211_01_T2_B8	12 December 2010			
LE07_L1GT_060114_20111113_20161205_01_T2_B8	13 November 2011			
LE07_L1GT_060114_20111215_20161204_01_T2_B8	15 December 2011			
LE07_L1GT_061114_20121208_20161128_01_T2_B8	8 December 2012			
LC08_L1GT_059114_20131103_20170428_01_T2_B8	3 November 2013	Landsat 8	OLI/ TIRS	15 m
LC08_L1GT_058114_20131214_20170427_01_T2_B8	14 December 2013			
LC08_L1GT_062113_20141229_20170415_01_T2_B8	29 December 2014			
LC08_L1GT_060114_20151218_20170331_01_T2_B8	18 December 2015			
LC08_L1GT_059114_20161127_20170317_01_T2_B8	27 November 2016			
LC08_L1GT_219130_20161214_20170316_01_T2_B8	14 December 2016			
LC08_L1GT_062113_20171119_20171205_01_T2_B8	19 November 2017			
LC08_L1GT_061114_20171230_20180103_01_T2_B8	30 December 2017			
LC08_L1GT_060114_20181124_20181124_01_RT_B8	24 November 2018			
LC08_L1GT_060114_20191127_20191127_01_RT_B8	27 November 2019			
LC08_L1GT_061114_20200206_20200211_01_T2_B8	6 February 2020			

Table S2. Ice thickness radar lines used to compare with hydrostatically derived ice thickness values.

Source	PST (project-season-track)
IceBridge HiCARS 2 L2 Geolocated Ice Thickness	DVG/JKB2e/Y05a
	DVG/JKB2e/Y10a
	DVG/JKB2e/Y14a
	DVG/JKB2e/Y18a
	DVG/JKB2e/X15a
	DVG/JKB2e/X16a
	DVG/JKB2e/X17a
	DVG/JKB2e/X17b

Table S3. Reference Elevation Model of Antarctica (REMA) 2m strip DEM IDs used in this study.

Strip DEM ID	Date
WV01_20111118_1020010016900B00_1020010017188D00_seg1_2m	18 November 2011
WV01_20111119_1020010018C1BC00_10200100181C2D00_seg2_2m	19 November 2011
WV01_20111127_1020010017852500_1020010016B88700_seg1_2m	27 November 2011
WV01_20111210_10200100178A7B00_10200100174F7200_seg1_2m	10 December 2011
WV01_20120220_1020010019ABB700_102001001AA93400_seg1_2m	20 February 2012

Table S4. Model run number, sheet conductivity, and channel conductivity values for the GlaDS sensitivity tests.

Model run number	Sheet conductivity ($m^{3/2}$ $kg^{-½}$)	Channel conductivity ($m^{3/2}$ $kg^{-1/2}$)
1	1×10^{-3}	1×10^{-1}
2	1×10^{-3}	5×10^{-1}
3	1×10^{-3}	5×10^{-2}
4	1×10^{-3}	5×10^{-3}
5	1×10^{-4}	1×10^{-1}
6	1×10^{-4}	5×10^{-2}
7	1×10^{-4}	5×10^{-3}
8	1×10^{-5}	5×10^{-3}
9	5×10^{-5}	5×10^{-3}

Table S5. Antarctic polar stereographic coordinates for channel locations at the grounding line, and channel discharge. Discharge (m^3 s^{-1}) is for each individual model run and average discharge (m^3 s^{-1}) is for individual channels. Sensitivity parameters for model runs are in Table S4.

Channel coordinates (x, y)	Model run number	Discharge (m^3 s^{-1})	Average discharge (m^3 s^{-1})
518597.5009, -1521484.771	6	0.15	0.17
	9	0.20	
	5	0.15	
520844.2546, -1520209.556	6	0.15	0.15
	7	0.22	
	2	0.16	
	3	0.13	
	4	0.11	
	5	0.15	
	1	0.14	
521676.2293, -1519909.872	7	0.10	0.10
522490.8564, -1519574.29	2	0.16	0.13
	5	0.10	
525648.4318, -1516109.904	2	0.12	0.12
526229.9308, -1514587.615	2	0.19	0.19
524984.9628, -1510434.794	6	0.15	0.43
	2	0.36	
	3	0.62	
	4	0.46	
	5	0.17	
	1	0.80	
524223.5313, -1509390.227	6	4.83	3.85
	7	4.33	
	2	3.96	
	3	2.55	
	4	1.76	
	8	5.11	
	9	4.52	
	5	4.97	

	1	2.59	
523954.9948, -1509070.482	2	0.15	0.31
	3	0.31	
	4	0.41	
	8	0.19	
	1	0.48	
523404.9763, -1508407.365	7	0.12	0.28
	3	0.33	
	4	0.46	
	1	0.22	
523057.6169 -1508133.485	4	0.17	0.17
522710.2575 -1507859.605	3	0.15	0.13
	1	0.11	